




Article

Water–Rock Interactions Driving Groundwater Composition in the Pra Basin (Ghana) Identified by Combinatorial Inverse Geochemical Modelling

Evans Manu ^{1,2,*} , Marco De Lucia ¹  and Michael Kühn ^{1,2} 

¹ GFZ German Research Centre for Geosciences, Fluid Systems Modelling, Telegrafenberg, 14473 Potsdam, Germany; delucia@gfz-potsdam.de (M.D.L.); michael.kuehn@gfz-potsdam.de (M.K.)

² Institute of Geosciences, University of Potsdam, Karl-Liebknecht-Str. 24-25, 14476 Potsdam, Germany

* Correspondence: evans.manu@gfz-potsdam.de

Abstract: The crystalline basement aquifer of the Pra Basin in Ghana is essential to the water supply systems of the region. This region is experiencing the ongoing pollution of major river networks from illegal mining activities. Water management is difficult due to the limited knowledge of hydrochemical controls on the groundwater. This study investigates its evolution based on analyses from a previous groundwater sampling campaign and mineralogical investigation of outcrops. The dominant reactions driving the average groundwater composition were identified by means of a combinatorial inverse modelling approach under the hypothesis of local thermodynamical equilibrium. The weathering of silicate minerals, including albite, anorthite, plagioclase, K-feldspar, and chalcedony, explains the observed median groundwater composition in the transition and discharge zones. Additional site-specific hypotheses were needed to match the observed composition of the main recharge area, including equilibration with carbon dioxide, kaolinite, and hematite in the soil and unsaturated zones, respectively, and the degradation of organic matter controlling the sulfate/sulfide content, thus pointing towards kinetic effects during water–rock interactions in this zone. Even though an averaged water composition was used, the inverse models can “bridge” the knowledge gap on the large basin scale to come up with quite distinct “best” mineral assemblages that explain observed field conditions. This study provides a conceptual framework of the hydrogeochemical evolution for managing groundwater resources in the Pra Basin and presents modelling techniques that can be applied to similar regions with comparable levels of heterogeneity in water chemistry and limited knowledge of aquifer mineralogy. The combinatorial inverse model approach offers enhanced flexibility by systematically generating all plausible combinations of mineral assemblages from a given pool of mineral phases, thereby allowing for a comprehensive exploration of the reactions driving the chemical evolution of the groundwater.

Keywords: combinatorial inverse modelling; thermodynamic equilibrium concept; water–rock interactions; PHREEQC; RedModRphree



Citation: Manu, E.; De Lucia, M.; Kühn, M. Water–Rock Interactions Driving Groundwater Composition in the Pra Basin (Ghana) Identified by Combinatorial Inverse Geochemical Modelling. *Minerals* **2023**, *13*, 899. <https://doi.org/10.3390/min13070899>

Academic Editor: Giovanni Mongelli

Received: 14 May 2023

Revised: 24 June 2023

Accepted: 29 June 2023

Published: 30 June 2023



Copyright: © 2023 by the authors. Licensee MDPI, Basel, Switzerland. This article is an open access article distributed under the terms and conditions of the Creative Commons Attribution (CC BY) license (<https://creativecommons.org/licenses/by/4.0/>).

1. Introduction

The Pra Basin is one of Ghana’s basins with high economic importance. Mineral resources, including gold, bauxite, iron, manganese, diamonds etc., mainly occur there. Several activities, such as large and small-scale plantations, fishing, and illegal mining, are pervasive. These economic activities alter the vegetation and have negatively impacted the water resources [1–7], especially surface waters. This situation has put much stress on the groundwater resource that the people rely upon for their water supply. However, the groundwater quality and geochemical controls on the regional scale are not well studied.

For this reason, Manu et al. [1] carried out a regional field study to assess the quality and characterized the hydrogeochemical properties of the groundwater. The main findings of their study, based on classical interpretations using bivariate ion plots and statistical

analysis, include the following: (1) the groundwater is generally of excellent quality for drinking and irrigation, (2) three spatial associations exist, which define the flow regime in the basin based on elevation differences, (3) the composition of the groundwater evolves along the hypothetical flow path from Ca–HCO₃ to Na–HCO₃ and finally to Na–Cl water types, (4) the water–rock interaction is the mechanism that controls the dissolved ion concentrations, and (5) silicate weathering, carbonate dissolution, and ion exchange are plausible chemical processes governing the groundwater composition. In a related study, Loh et al. [8] used the stable isotopes data in the Lake Bosumtwi area and highlighted that (1) the groundwater originates from precipitation, and (2) the infiltrating water in the unsaturated zone is affected by evaporation before reaching the saturated zone. Their findings are akin to the previous studies conducted at the local scale at different locations in the Pra Basin [9–11]. The research results presented so far have mainly offered qualitative interpretations without focusing on the quantitative aspects of the chemical reaction processes. As a result, there is a lack of accurate information about the dissolved or precipitated minerals responsible for the chemical development of the groundwater. Furthermore, the lack of a functional conceptual model for reaction pathways hampers our understanding of how groundwater chemical composition changes along its flow path. To fill these gaps, this study uses geochemical models to provide a more comprehensive understanding of the key hydrochemical reactions driving the groundwater evolution.

Geochemical models are essential for analyzing chemical reactions in natural geological systems such as rocks, minerals, and fluids. These models are based on the principles of thermodynamics, kinetics, mass balance, and fluid dynamics, and they help to quantify geochemical processes, including dissolution, precipitation, sorption, and ion exchange, which control groundwater chemical evolution [12,13]. Approaches used to study these processes include inverse and forward modelling. Classical inverse geochemical modelling utilizes mass balance to quantify the amounts of reactions of predetermined phases to account for chemical changes observed between two end-member solutions [14]. This approach involves defining the known chemical composition of the initial and final solutions and specifying the reacting mineral phases; the model determines the set of mole transfers for the mineral phases that explain the evolution of the final water composition [15], irrespective of thermodynamical constraints. Conversely, forward modelling applies local thermodynamic equilibrium to an initial solution in contact with a determined mineral assemblage to predict the final solution and, thus, the amounts of reacting phases needed to reach a local equilibrium [15].

Several software packages, including PHREEQC [16], Geochemist Workbench [17], TOUGHREACT [18] etc., are available to implement geochemical models. Among these codes, PHREEQC [16] is one of the most widely used codes to perform geochemical simulations. Its popularity is attributed to factors such as the availability of the source code, its widespread usage among users, and its extensive documentation. Recently, De Lucia and Kühn [19] proposed a geochemical and reactive transport modelling package (RedModRphree) that leverages the R programming interface to establish PHREEQC geochemical simulations. The power of the RedModRphree lies in its flexibility to program algorithms associated with geochemical models, including error and sensitivity analysis, parameter calibration and optimization, statistical modelling, and thermodynamic database manipulation [19].

In this study, we utilized geochemical simulations to investigate the chemical evolution of groundwater in the highly heterogeneous geochemical environment of the Pra Basin. Our modelling approach started by defining a conceptual reaction path model based on the findings from the previous works enumerated above. Three conceptual flow paths were adopted following the results of Manu et al. [1] and Loh et al. [8]. A combinatorial inverse modelling technique (Section 2.7.1) was employed as an exploratory approach to identify plausible mineral assemblages whose thermodynamical equilibria could explain the observed composition of groundwater along the flow regime. Unlike classical inverse modelling, which relies solely on mass balance, this technique operates under the

assumption of local thermodynamic equilibrium. The best matching mineral assemblages were further calibrated using conceptualized reaction path models that were depicted to include, e.g., the influence of unsaturated zone. Based on the model results, a potential hydrogeochemical evolution model was obtained that identifies the driving hydrochemical processes along the groundwater flow in the Pra Basin. The developed conceptual framework serves as a foundation for further investigation and analysis of the hydrogeochemical dynamics in the basin.

2. Materials and Methods

2.1. Study Area

The study area consists of the two sub-basins including the Birim and the Lower Pra of the main Pra Basin, located in the southern parts of Ghana. The geographical location, physical setting, climate and major economic activities in the basin are described in Manu et al. [1].

2.2. Geological Setting

The study area is dominated by two rock formations (Figure 1): the Birimian Supergroup and the Cape Coast granitoid [20]. The Tarkwain Rock Formation occupies smaller portions and is mostly found on the eastern and western edges of the study domain. The Birimian rocks predominantly underlie the northern portions and the Cape Coast granitoid south of the basin. A detailed study of the mineral and rock composition of the Birimian, Tarkwain, and Cape Coast granitoid rock formations has been copiously discussed in the literature [21–23]. The Birimian metasediments consist of phyllite, schists, greywacke, weakly metamorphosed tuffs, feldspathic sandstones, and Mn- and Si-rich chemical sediments [22,24,25]. The phyllites have been found to contain pyrite and finely divided carbonaceous matter [26]. Available data suggest that the phyllite and meta-greywackes contain significant amounts of calcite (over 15% in some cases) in the Birimian metasediments [27]. High biotite and plagioclase minerals have also been reported in the Birimian rocks [27]. The Tarkwaian rocks consist of sandstones, conglomerates, and argillites, which constitute a clastic sequence of arenaceous and argillaceous sediments [22]. Most of the southern parts of Ghana are underlain by the Cape Coast granitoid [22,28]. The pegmatites of the Cape Coast granites occur as dykes with feldspars, quartz, and micas as the dominant mineral composition [22]. The Cape Coast type granitoid also comprises granitic to quartz dioritic gneiss, which changes from medium-grained, foliated biotite quartz diorite gneiss to horn-blended quartz–diorite gneiss [29].

2.3. Hydrogeologic Conditions

The study area falls within the Crystalline Basement Granitoid Complex and the Birimian Province in Ghana. In general, the rocks are inherently impermeable; however, secondary porosity results from fractures and faults that control groundwater movement [26]. The hydrogeological units consist primarily of a saprolite overlain by duricrust, saprock, and underlying bedrock. The saprolite is deeply weathered and consists of clay or silt. The saprock is oxidized and forms the transition zone between the saprolite and the bedrock. Groundwater occurs in two distinct hydrogeological units comprising the overburden and the bedrock. The bedrock consists of granitoid and Birimian rocks, which vary in thickness and fracture intensity [26].

2.4. Field Work

Fieldwork was undertaken to sample rocks for mineralogical studies. Figure 1 shows the geological map of the study area with the outcrop locations. A total of seven representative samples were collected comprising four from the Birimian Supergroup and three from the Cape Coast granitoid formation. The description of the measurements and the mineralogical composition identified by the petrographic thin section analyses are described in Manu et al. [30].

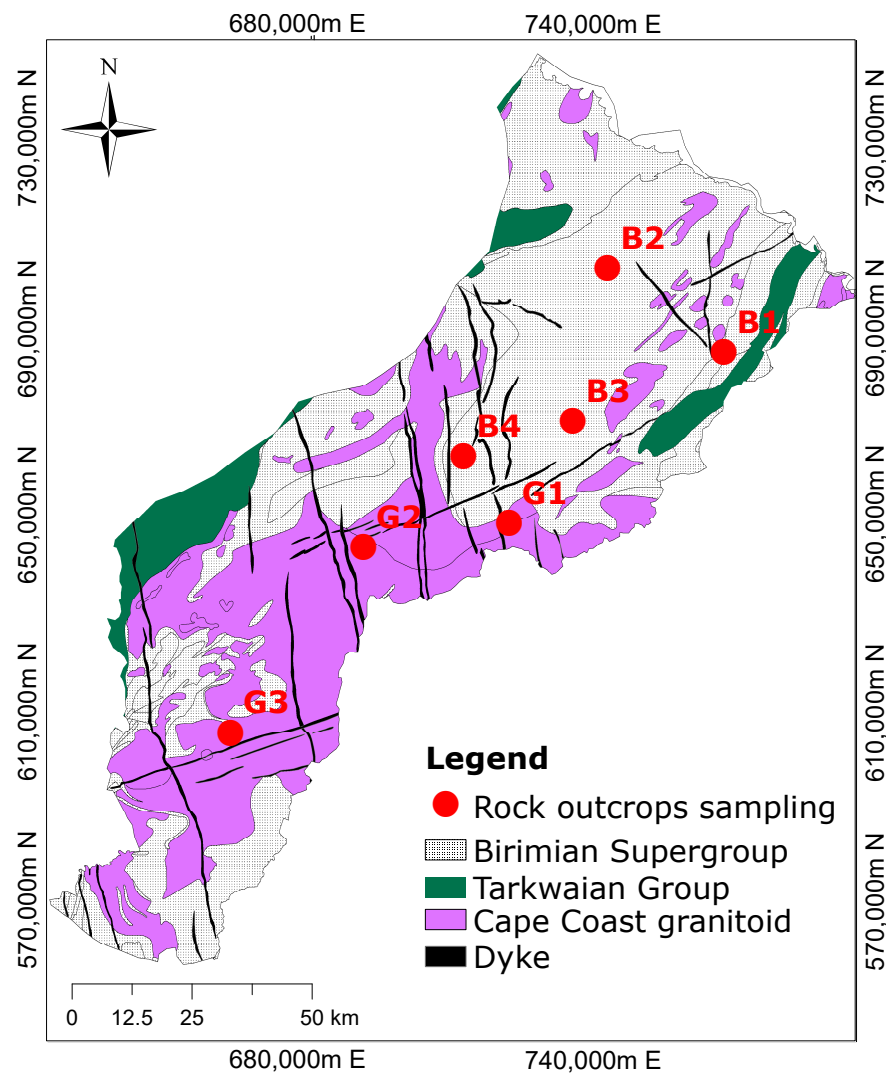


Figure 1. Geological map showing the dominant rock formations and the sampling locations. The Birimian rocks are composed of metasediments, while the Cape Coast granitoid is composed of granite, and the Dyke is made of dolerite (modified after Manu et al. [1]).

2.5. Modelling Input Data Sources

The data used for the geochemical modelling include major ion chemical compositions from rainwater and groundwater samples, as well as mineralogical information determined by thin section petrography analysis. Three sets of information were required for model setup: (1) the initial solution—in our case, we used chemical data from the rainwater, (2) the final solution, which is the groundwater composition, and (3) the mineralogical information.

In this study, the hydrochemical data of the rainwater (Table 1) in close vicinity to the Pra Basin were taken from Akoto et al. [31] and used as the initial solution. Chemical parameters such as pH, Na^+ , K^+ , Ca^{2+} , Mg^{2+} , HCO_3^- , Cl^- , and SO_4^{2-} were used for the starting aqueous components in our modelling. In their study, Loh et al. [8] estimated the evaporation rate of rainwater before groundwater recharge to be between 54% and 60%. In view of this, the initial solution was simulated by evaporating rainwater until the chloride concentration measured in the groundwater was reached. In that way, chloride was used as a conservative tracer unaffected by the chemical reaction processes. This assumption is reasonable, as there is no evidence of halite in the underlying geology to dissolve and alter the Cl^- concentration of the infiltrating water. The final chemical composition of the evaporated rainwater was then used as the initial solution for the combinatorial and reaction path modelling.

Table 1. Hydrochemical data from rainwater and groundwater used for the modelling. The rainwater (RW) and groundwater (comprising northern, central, and southern) data were adopted from Akoto and Adiyiah [32] and Manu et al. [30]. ND denotes not determined.

Parameter	Units	RW	Median			Range		
			Northern	Central	Southern	Northern	Central	Southern
pH	-	4.7	6.5	6.1	6.0	5.9–7.0	5.6–6.4	5.3–6.4
Temp	°C	ND	28.1	28.4	29	26.0–29.0	28.1–29.6	27.8–31.0
Na ⁺	mg/L	0.4	11.9	17.1	44.3	3.1–32.4	9.2–21.8	16.4–67.4
K ⁺	mg/L	0.7	0.7	3.7	6.1	0.3–8.2	0.4–6.3	1.2–16.3
Ca ²⁺	mg/L	0.8	26.4	7.2	14.8	12.6–51.5	2.1–13.5	3.1–66.0
Mg ²⁺	mg/L	0.3	6.4	2.5	7.2	1.6–12.8	0.9–4.6	1.5–29.4
HCO ₃ ⁻	mg/L	6.7	108.5	3.7	28.0	37.8–191.0	29.3–67.1	5.0–134.0
Cl ⁻	mg/L	4.5	8.4	12.7	58.1	2.4–49.0	6.0–21.5	17.5–196.7
SO ₄ ²⁻	mg/L	11.1	1.1	1.6	8.6	0.4–66.0	0.1–4.3	1.6–99.4
Fe(total)	mg/L	ND	0.2	0.01	0.02	0.008–0.8	0.001–0.2	0.006–0.09
SiO ₂	mg/L	ND	23.9	23.4	17.5	7.2–33.7	13.6–37.3	11.8–29.7

The hydrochemical data of the groundwater from Manu et al. [1] were adopted in the present study. The median ion concentrations shown in Table 1 of the samples were taken to represent each of the three zones (Figure 2) along the flow path from the recharge to the discharge zone. The rationale for using the median as the final representative composition was to minimize the error introduced by outliers and the natural variability in the water samples [33]. The chemical parameters of groundwater considered for the modelling included pH, Na⁺, K⁺, Ca²⁺, Mg²⁺, HCO₃⁻, Cl⁻, SO₄²⁻, Fe, and SiO₂.

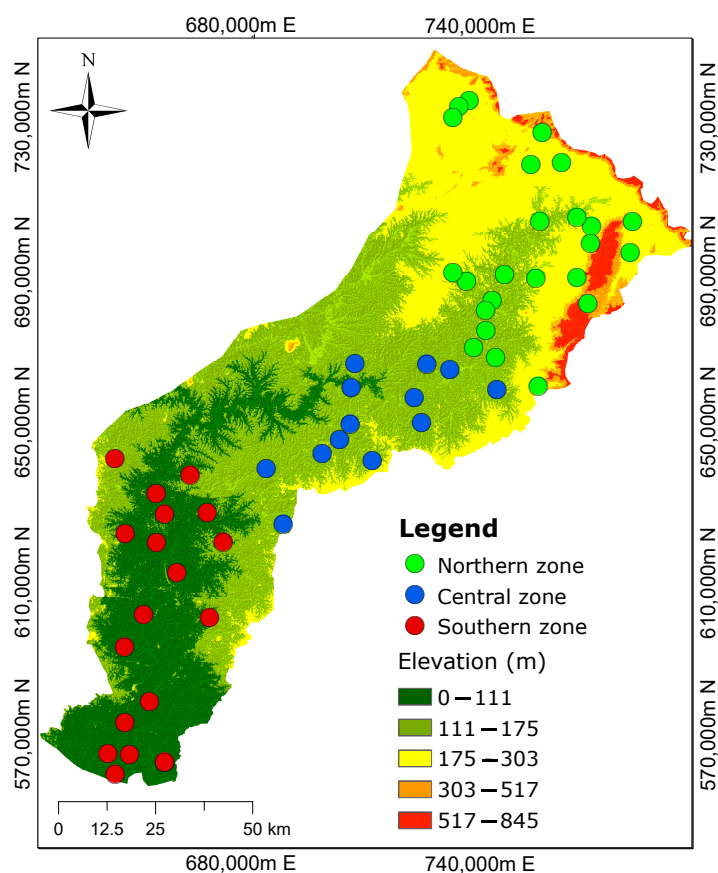


Figure 2. Three demarcated zones from the previous study by Manu et al. [1] show the spatial distribution of groundwater sampling sites. The northern zone is characterized by high elevations, while the southern zone has low elevations. The groundwater flow is assumed to mimic the topography.

The mineral phases were selected from a petrographic study performed on outcrop samples by Manu et al. [30]. Photomicrographs showing the mineralogical and textural features of the rock samples are presented in Figure 3. The mineralogical composition of the Birimian rocks underlying the northern zone consists of biotite, chlorite, quartz, sericite, minor K-feldspar, and calcite (Figure 3B1–B3). Iron oxides are visible in hand specimens. Biotite has significantly altered to chlorite, while the K-feldspar has altered into sericite. The granitoid is located principally over the southern zone and comprises quartz, plagioclase, K-feldspar, muscovite, and biotite with accessory chlorite and sericite (Figure 3G1–G3). In our study, the presence of albite was confirmed through XRD analysis, while plagioclase was identified through thin section analysis. Additionally, we assumed the presence of anorthite, the calcium end-member of plagioclase, in the system. The mineral phases considered for combinatorial inverse modelling along the three flow paths included primary albite, anorthite, plagioclase, phlogopite, K-mica, K-feldspar, $\text{Fe}(\text{OH})_3$, and calcite, as well as secondary kaolinite, Ca-montmorillonite, chlorite (14A), quartz, pyrite, and chalcedony. Here, the primary and secondary minerals were considered as reactants and products, respectively.

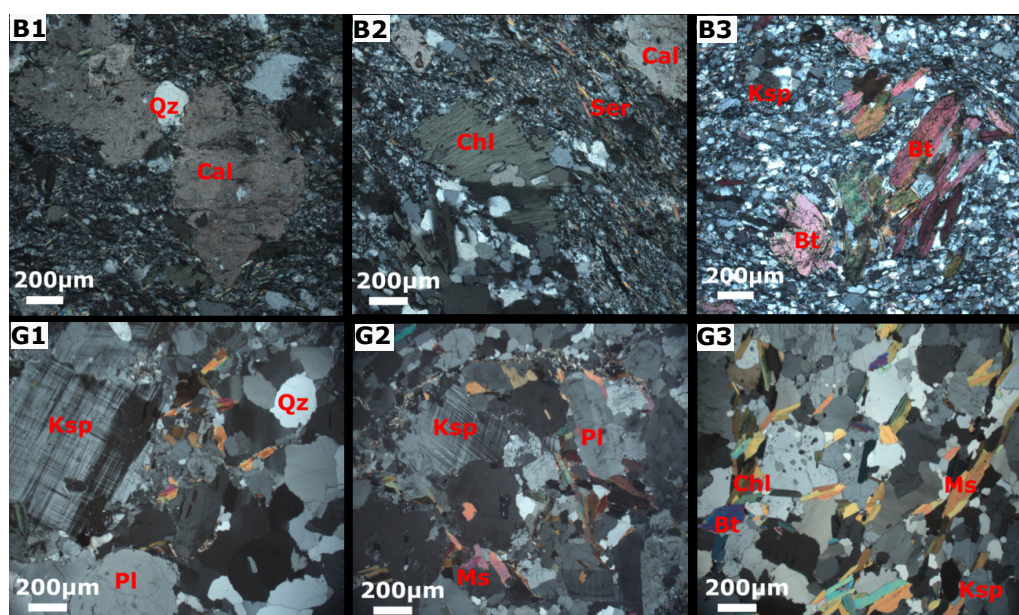


Figure 3. Thin sections of rock outcrops (adopted from Manu et al. [30]). The first row shows the mineralogy of the Birimian metasediments (B1,B2,B3), including quartz (Qz), biotite (Bt), K-feldspar (Ksp), sericite (Ser), chlorite (Chl), and calcite (Cal). The second row shows the mineral composition of the granitoid (G1,G2,G3) comprising quartz (Qz), K-feldspar (Ksp), plagioclase (Pl), muscovite (Ms), and biotite (Bt).

2.6. Geochemical Code and Thermodynamic Data

In this study, the geochemical modelling code PHREEQC [16], was chosen for the numerical simulations, with the `phreeqc.dat` as the selected database. The underlying reasons for choosing PHREEQC are threefold: (1) code availability, (2) wider user coverage, and (3) adequate documentation.

Minerals such as plagioclase, biotite, and muscovite were originally not included in the `phreeqc.dat` database. Biotite or “black mica” was introduced in the model as the Mg end-member phlogopite, adopted from the `thermodem` thermodynamic database [34]. Muscovite or “white mica”, was introduced as K-mica. For the plagioclase, a fixed stoichiometry of 0.38 Ca/0.62 Na was assumed. Its equilibrium constant was estimated by weight averaging the equilibrium constants of the two end-members, anorthite and albite, using their definitions in `phreeqc.dat`. The chemical equations, along with the thermodynamic equilibrium constants of the added phases in the `phreeqc.dat` database, are presented in

Table A1 (Appendix A). The RedModRphree package [19] was used to set up and perform the combinatorial screening and the calibration of the reaction path models described in the next section. For more detailed information about the RedModRphree setup, see De Lucia and Kühn [19].

2.7. Geochemical Modelling

2.7.1. Combinatorial Inverse Modelling Approach

A multi-step inverse modelling approach was devised to successively integrate field observations into models and then to calibrate the latter with known geochemical constraints. Notably, in a preliminary combinatorial inverse approach, all possible mineral assemblages drawn from a pool of potential minerals were screened under local thermodynamic equilibrium conditions aimed at identifying the mineral assemblage that would best explain the changes in composition along the flow path of the groundwater. This was a different goal than with classical inverse geochemical models, which consist rather in computing the amount of mole transfer from a predetermined mineral assemblage [35].

Three hypothetical flow paths were defined based on the cluster analysis conducted by Manu et al. [1]. Flowpath I includes rainwater as the starting point and the northern zone groundwater as the final solution. Flowpath II represents two end-member solutions, the northern and central zones, while Flowpath III represents the water transfer from the central and to the southern zones. The median ion concentrations of the groundwater samples within the three zones postulated by Manu et al. [1] were retained as representative and used as target concentrations to rank all computed equilibrium models.

The modelling procedure begins with the definition of the starting solution, which represents evaporated rainwater and has chemical concentrations stated in mol/kgw. The temperature is assumed to be 25 °C, which corresponds to the average temperature of groundwater samples collected in the study region. Certain components, such as iron and silica, were not originally present in the rainfall composition and were labelled as NA (not applicable) to guarantee consistency between the target groundwater concentrations and the predicted results.

The simulation used the `phreeqc.dat` database, which was adjusted to include minerals such as phlogopite and plagioclase, as well as organic matter. Target concentrations, representing the groundwater elemental composition in the northern, central, and the southern zones, were specified in order to compare the modelled results with the observed concentrations. The primary and secondary minerals were defined to dissolve or precipitate when present in the groundwater solution.

The simulation was programmed to generate all potential combinations of 3 to 8 mineral phases drawn from predetermined pools of primary and secondary minerals. Each resulting mineral assemblage was then considered at equilibrium with the initial water, and the final total elemental concentrations of the modelled solutions were ranked by their discrepancy to the target solution. We assumed that any mineral combination resulting in a model solution would be plausible for explaining the observed composition.

In this study, a pool of 14 mineral phases comprising primary albite, anorthite, plagioclase, phlogopite, K-feldspar, K-mica, $\text{Fe}(\text{OH})_3$, and calcite, as well as secondary kaolinite, Ca-montmorillonite, chlorite, quartz, pyrite, and chalcedony, were used as the reactants and products for the combinatorial inverse modelling. Pyrite was not included along Flowpath III, as there was no evidence of its presence in the granitoid formation.

Given the large pool of mineral phases, several thousand models were generated. Here, a maximum allowable threshold reactivity of 0.5 mol/kgw was applied to eliminate models where two competing mineral phases or proxies for the same element were present in the system. The reason for this is that, in the case of a complete dissolution of a mineral phase leading to the precipitation of large amounts of a stable phase, physically unrealistic results would be obtained.

The ensemble of computed equilibrium models was compared to the observed concentration range of the aqueous groundwater components, and models that did not fall within

the observed concentration ranges were removed. Due to the ill-posed nature of inverse models, there can be multiple solutions that fit the observed data. Therefore, we utilized the relative root mean square error (RRMSE) (Equation (1)) of all the aqueous components of the equilibrium models with respect to the target concentrations in order to rank the matches obtained.

$$\text{RRMSE} = \sqrt{\frac{1}{n} \sum_{i=1}^n \left(\frac{y_i - \hat{y}_i}{y_i} \right)^2}, \quad (1)$$

where i represents the respective ions, y_i represents the observed aqueous concentrations, \hat{y}_i represents the simulated aqueous components, and n is the total number of elements to be matched.

Finally, the contingencies for each mineral phase contained in the 50 best-matching models were calculated. The rationale for the frequency calculations is that, when a mineral phase is present in many high-ranked models, the probability of identifying a reactive mineral phase is greater than the minerals not represented in the same ensemble.

2.7.2. Calibration Based on Reaction Path Scheme

Based on the combinatorial inverse modelling results, the mineral assemblages identified as most probable were further calibrated according to the conceptual reaction path model shown in Figure 4. The reaction path modelling was implemented through a five-step approach, as discussed in the following.

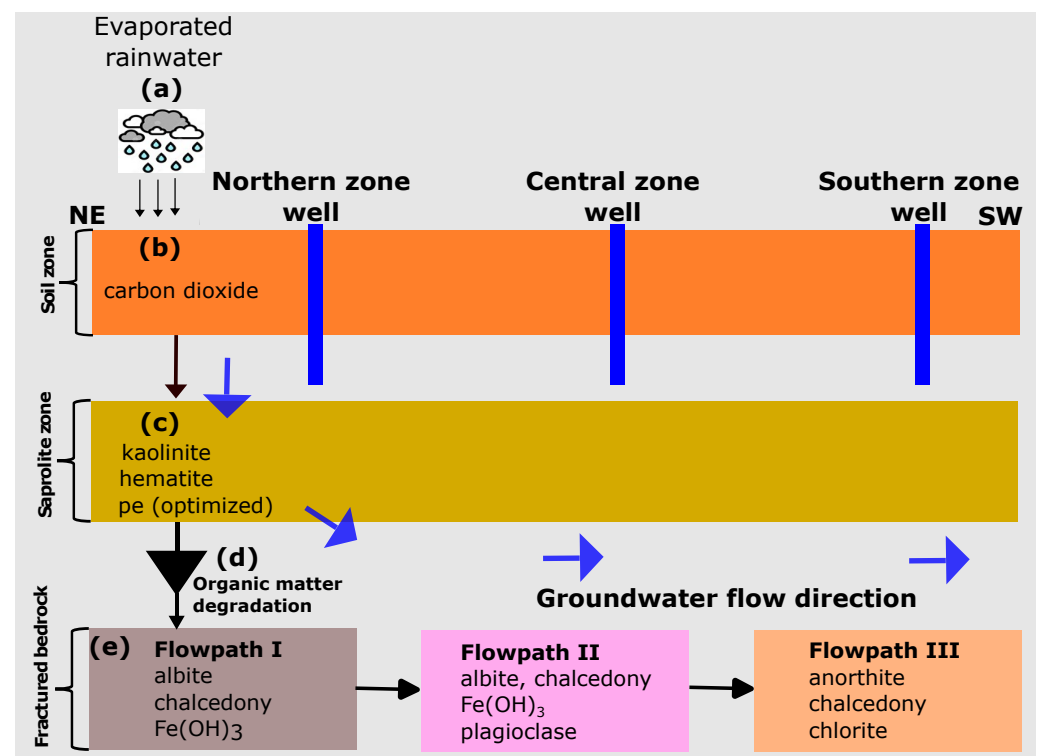


Figure 4. Conceptual reaction path models considering the rainwater origin of the groundwater. The northern zone is assumed to be the recharge area at high elevations. Vertical flow in the central and southern zones is assumed to have no significant impact on groundwater chemical evolution.

In step (a), the rainwater composition was subjected to evaporation using the Cl^- concentration in the northern zone groundwater as the target concentration. The final solution after evaporation was saved and used as the starting solution for the reaction path modelling.

Step (b) involved the equilibration of the evaporated solution with CO₂ in the topsoil. Here, we performed a trial and error calibration by adjusting the partial pressure of CO₂ until a reasonable match with the HCO₃⁻ in the observed concentration was achieved. This approach was deemed necessary due to the lack of soil measurements for carbon dioxide (CO₂) in the current investigation.

In step (c), the solution from step (b) was equilibrated with kaolinite and hematite. The saprolite is deeply weathered and consists of clay and silty clay. The uppermost part comprises red laterite clay and duricrust dominated by cemented iron oxides and silica nodules. In an ideal scenario, the release of Al and Fe into the solution is primarily attributed to primary silicate and Fe-containing minerals. However, to simplify the model, we utilised secondary minerals, namely kaolinite and hematite, to estimate the equilibrium quantities of Al and Fe in the solution. The redox potential of the water in the unsaturated zone was then optimized in order to control the Fe concentration. We used the trial-and-error method to optimize the redox (pe) of the infiltrating water in the unsaturated zone. This method was used because no redox potential (pe) measurements were carried out in the current study. The numerical values determined by manual calibration offered a preliminary estimate of the prevailing redox conditions in the groundwater system.

In step (d), we integrated the organic matter degradation reaction into the batch model to control the sulphate/sulphide content in the groundwater. Based on the hypothesis that organic matter present in the groundwater system under anaerobic conditions is responsible for the lower SO₄²⁻ concentrations, we also assumed that iron oxides present in the metasediments underwent further reactions with H₂S, which is formed during the decomposition of the organic matter. These reactions result in the formation of iron sulfide minerals, particularly pyrite, as observed in our study. To represent the organic matter, we used the hypothetical compound CH₂O, as suggested by Pitkaenen et al. [36]. Since the organic matter content in the soil was not measured, we adjusted the CH₂O values until the observed sulphate content in the groundwater was matched.

In step (e), the solution from step (d) was equilibrated with the determined aquifer mineralogy in the three zones identified by combinatorial inverse modelling.

3. Results

3.1. Mineral Assemblages Identified from the Combinatorial Inverse Modelling

Given the large pool of mineral phases, 12,805 unique models each were generated for Flowpath I and II, and 7007 models were generated for Flowpath III. However, by implementing a threshold reactivity of 0.5 mol/kgw, only 11,788 models for Flowpath I, 11,785 models for Flowpath II, and 6370 models for Flowpath III converged to a physically meaningful solution.

Combinatorial inverse modelling provided sets of potential model solutions that fell within the range of the observed aqueous compositions of the groundwater. The RRMSE values obtained for the 50 best-matching simulations ranged from 2.769 to 2.783 with a mean of 2.777 for Flowpath I, from 0.433 to 0.472 with a mean of 0.458 for Flowpath II, and from 0.329 to 0.395 with a mean of 0.365 for Flowpath III. Based on the RRMSE values, Flowpath I, which comprises the evolution from precipitation to the northern zone groundwater, had the highest RRMSE values exhibiting larger deviations from the median concentrations. In the case of Flowpath I, the inverse equilibrium calculation could not produce a model that matched all the measured aqueous components in the groundwater (northern zone). In general, Ca²⁺, Mg²⁺, HCO₃⁻, Cl⁻, SO₄²⁻, and SiO₂ showed fairly good matches between the modelled and the median concentrations adopted in our simulation. Ions including Na⁺, K⁺, and Fe(total) showed significant variations from the median concentrations, although several models were within the measured compositional range. Figure 5A depicts the mineral frequency distribution of the best-matching 50 equilibrium models. The most frequently occurring minerals included Fe(OH)₃, chalcedony, plagioclase, pyrite, chlorite, and albite. The best-matched equilibrium simulation yielded three dominant mineral reactions: the dissolution of albite and Fe(OH)₃ and the precipitation of chalcedony. It

is important to highlight that this mineral assemblage is considered among the potential combinations in the various equilibrium models for further calibration using the reaction path models.

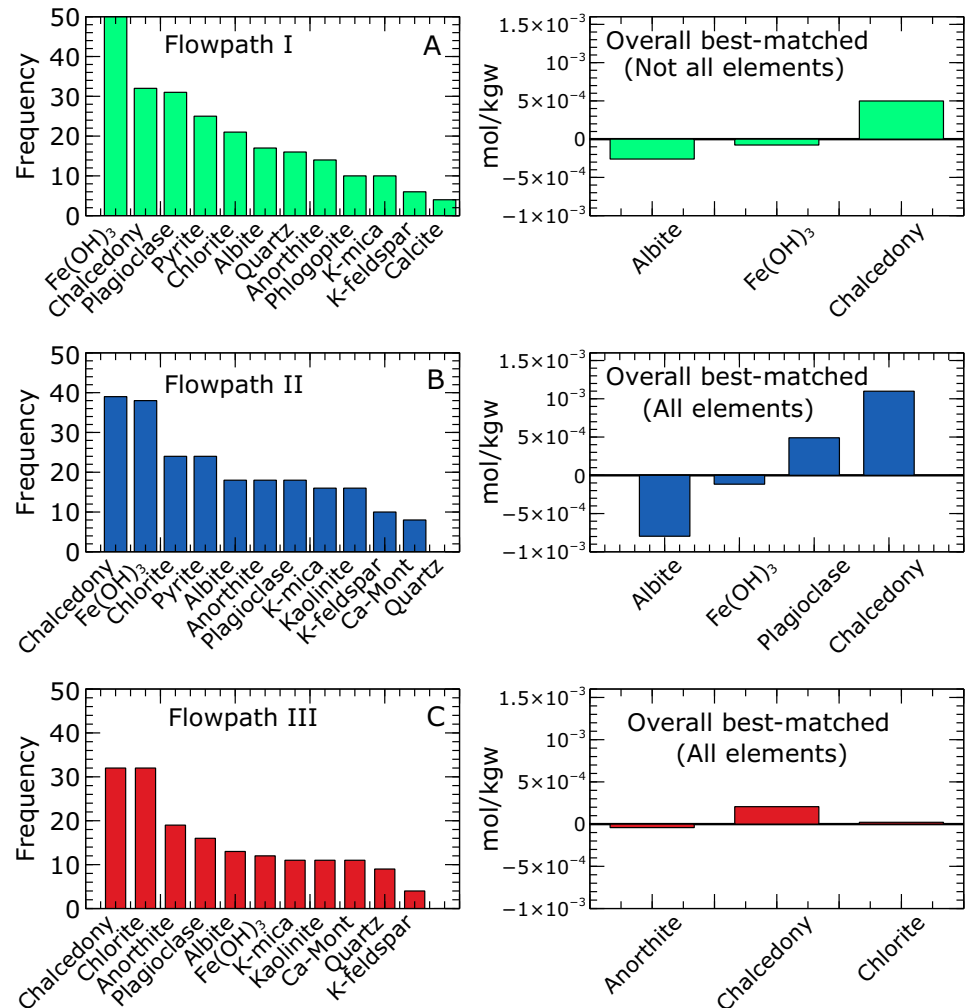


Figure 5. Frequency distribution of the 50 best inverse equilibrium models. For the northern zone (Flowpath I), no model matched all the aqueous components; however, the best simulations are shown in (A). Simulations matching all the measured aqueous components in the groundwater and mineral reactions for the overall best-matched for the central (Flowpath II) and southern zones (Flowpath III) are shown in (B,C), respectively. The minerals with a higher number of occurrences underscore the likelihood of a reactive mineral phase. Negative and positive mole transfers indicate mineral dissolution and precipitation, respectively.

For Flowpath II, the inverse equilibrium calculations yielded 188 simulations that matched the observed aqueous components. The mineral frequency distribution of the top 50 matching models is presented in (Figure 5B). The prevalent minerals found to be in equilibrium with the waters in the central zone were chalcedony, Fe(OH)₃, chlorite, pyrite, albite, and anorthite. The overall best equilibrium simulation revealed four dominant mineral reactions: the dissolution of albite and Fe(OH)₃ and the precipitation of plagioclase and chalcedony.

Regarding Flowpath III, the inverse equilibrium calculation produced 180 simulations that matched the observed aqueous components. The mineral frequency analysis (Figure 5C) performed on the top 50 matching models within the range of measured aqueous compositions revealed that chalcedony, chlorite, anorthite, and plagioclase were the most common minerals likely to be in equilibrium with the groundwater in the southern

zone. These mineral assemblages aligned with the predicted minerals in the overall best-matched solution. The overall best equilibrium model showed three dominant minerals: anorthite, chalcedony, and chlorite. Notably, anorthite was observed to dissolve, while chalcedony and chlorite precipitated as the system approached equilibrium.

3.2. Reaction Path Modelling

Reaction path modelling was applied to mimic the flow path of the water from the recharge area (northern zone) to the discharge zone (southern zone), thus getting into contact with the mineral assemblages deduced from the inverse equilibrium models. Figure 6a–c compare the observed and modelled concentrations of aqueous components resulting from subsurface reactions with aquifer materials in the three zones. Generally, all modelled concentrations fell within the range of the observed values. We found that the chemical evolution of the groundwater in the Pra Basin is driven by silicate weathering (albite, anorthite, plagioclase, chalcedony, and chlorite) and that the subsurface reaction path is sufficient to quantify groundwater composition along the flow regime from the recharge (northern zone) to the discharge area (southern zone).

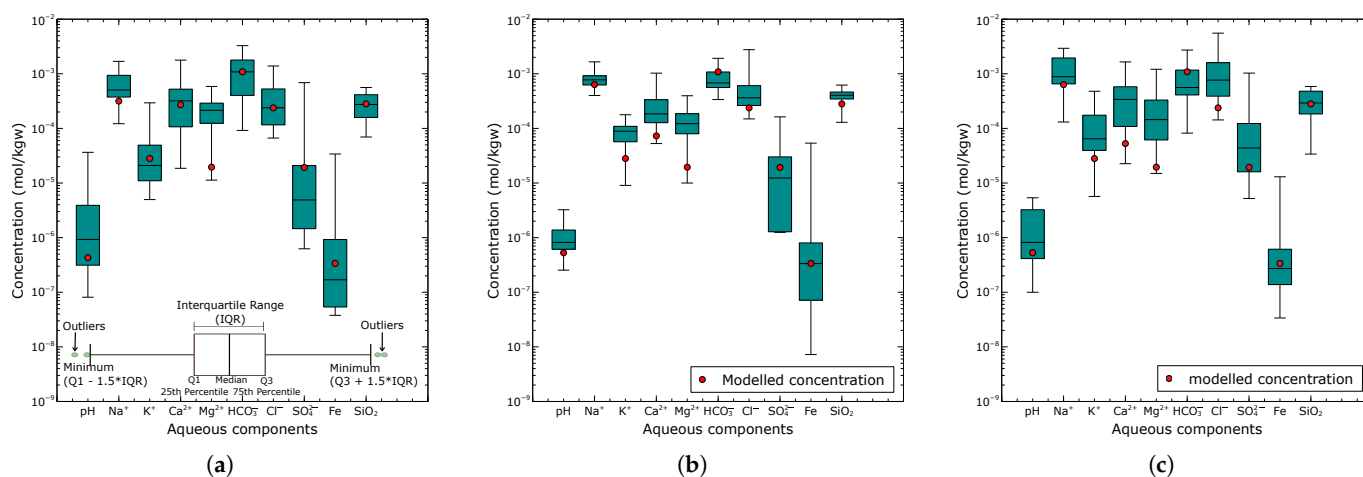


Figure 6. Comparison of the predicted aqueous groundwater components (red circles) from the reaction pathway calibration model and the range of observed composition (box plot) for the northern zone (a), central zone (b), and southern zone (c).

Figure 6a presents the modelled groundwater results for the northern zone based on the equilibration of the final calibrated rainwater with the mineral assemblage determined from the combinatorial inverse model along Flowpath I. The modelled concentrations of all aqueous components were within the interquartile range of the observed composition, except for Mg^{2+} , which showed significant deviations from the median. Notably, in our combinatorial inverse modelling, none of the equilibrium simulations matched all the observed aqueous components. Further calibration was required to model the northern zone groundwater, including considerations for rainwater evaporation, the equilibration of CO_2 in the soil zone, the equilibration of kaolinite and hematite, as well as redox optimization, in the unsaturated zone, and the degradation of organic matter. The rainwater underwent an evaporation rate of 47%, which doubled all ion concentrations until the chloride (Cl^-) concentration in the groundwater of the northern zone was reached. A partial pressure of $10^{-1.7}$ atm for CO_2 was considered significant in causing an increase in the HCO_3^- concentration of the water infiltrating the soil zone. Since no measurements were available for Fe and SiO_2 in the rainwater, the equilibration of hematite and kaolinite provided initial concentrations of 4.89×10^{-13} mol/kgw for Fe and 2.19×10^{-4} mol/kgw for SiO_2 , respectively, for the modelled groundwater. The redox potential (pe) was adjusted until a value of 3.5 was sufficient to produce a Fe concentration of 3.38×10^{-7} mol/kgw that matched the observed northern zone groundwater composition. This value represents

a plausible estimation of the redox state of the unsaturated zone process in the groundwater system in the northern parts of the area. Organic matter degradation results indicated that an estimated amount of 4.0×10^{-4} moles was sufficient to produce a SO_4^{2-} concentration in the range of the observed groundwater composition in the northern zone (recharge area).

Figure 6b shows the results of the modelled groundwater composition for the central zone (Flowpath II) compared with the observed compositional ranges. Among the simulated aqueous components, pH, Na^+ , HCO_3^- , Cl^- , SO_4^{2-} , Fe, and SiO_2 were closest to the observed median composition. In contrast, K^+ , Ca^{2+} , and Mg^{2+} showed relatively low values relative to the median. Changes in the redox conditions did not show any significant effect on the simulated water composition.

Figure 6c presents the modelled groundwater composition of the southern zone compared with the observed aqueous concentrations. The simulated aqueous concentrations were within the observed compositional range. All aqueous components, except K^+ , Ca^{2+} , Mg^{2+} , and Cl^- , showed minimal deviation from the median composition.

4. Discussion

The petrographic investigations on the outcrops showed the mineral composition of the rocks in the study area. Our simulation results indicate that the identified minerals are consistent with the general mineralogy of the Birimian metasedimentary rocks [22,25,37] and the Cape Coast granitoid [22,28]. In particular, our analysis indicates the alteration of primary minerals, such as biotite and K-feldspar, into secondary chlorite and sericite, which is consistent with previous studies [22,25]. The metasedimentary rocks were also found to contain some minor traces of calcite, which were believed to have formed from the metamorphism of the sediments. This is broadly consistent with observations by Yidana et al. [27], thus suggesting that the phyllite and metagreywacke associated with the metasediments contain about 15% or more calcite.

Our modelling results enabled the identification of plausible minerals and a likely reaction path model that controls the chemical evolution of the groundwater. To the best knowledge of the authors, this is the first time an attempt has been made to provide specific minerals that influence the chemistry of the groundwater rather than use the generalizations derived from the classical interpretations of the hydrochemical data that suggest silicate mineral weathering as the dominant mineral reaction in the study area [1,9,11]. In this study, we found that the mineral phases predicted by our modelling were consistent with petrographic analyses. However, we did notice a discrepancy between our modelling results and observations for the recharge zone (Flowpath I from rainwater to the northern zone). With our inverse equilibrium model, we found no possible matching solution, thereby indicating that the mineral reactions may not be in equilibrium and that kinetic processes may be responsible for the observed discrepancy. Nevertheless, within the simulated results, we could deduce the probable mineralogy consistent with the petrographic results of the outcrop samples. The overall best-matched modelled results showed the equilibration of albite, $\text{Fe}(\text{OH})_3$ and chalcedony in this zone. On the other hand, the central and the discharge zone (the other two Flowpaths II and III) resulted in distinct solutions that explain the observed water composition. This suggests that the reactions are predominantly controlled by thermodynamics in these zones. Our model outlines that, among the best-matched simulations, a frequency count can infer the most likely minerals that equilibrate with the groundwater. Groundwater migrating from the northern zone is likely to equilibrate with albite, plagioclase, $\text{Fe}(\text{OH})_3$, and chalcedony to produce the groundwater chemical composition of the central zone (Flowpath II). These predicted minerals are consistent with field data indicating the presence of primary albite and plagioclase in the rock formation. Similar results have been reported by Adiaffi et al. [38]. Water flowing from the central to the southern zone (Flowpath III) is equilibrated with anorthite, chalcedony, and chlorite.

Concerning our assumptions, and in particular those of thermodynamic equilibrium, we have to recognize that the northern recharge zone (Flowpath I) requires additional hy-

potheses and degrees of freedom in order for the calibration to agree with the observations. We argue that the formation water residence time in the rock was probably not long enough to reach equilibrium and that the reactions are kinetically controlled. Given this additional hypothesis, it was necessary to assess the influence of the infiltration processes in the soil and the unsaturated zone before the water entered the aquifer to interact with the rocks. We propose here that the excess HCO_3^- may arise from the reaction between CO_2 in the soil zone and the decomposition of organic matter, which could also account for the decrease in SO_4^{2-} concentration. In principle, the CO_2 generated through the respiration of plant roots in the soil zone reacts with water (H_2O) to generate a weak carbonic acid that dissociates and releases H^+ into the solution [39,40]. The presence of H^+ combines with the CO_3^{2-} complex to form HCO_3^- . In our study, adding this step resulted in a significant increase in HCO_3^- from 2.07×10^{-4} mol/kgw to 6.86×10^{-4} mol/kgw, which is well in line with the observed concentration. Regarding the additional SiO_2 , the equilibration of the water with kaolinite in the unsaturated zone accounted for this deviation. Adiaffi et al. [38] observed the same in the southeast of Ivory Coast in the subregion.

The reduction in sulfate concentration in the groundwater, relative to rainwater, is primarily driven by the degradation of organic matter. The initial solution (rainwater) used in our study shows a high sulfate content and lower pH, which was attributed to the evaporation and oxidation of sulfur dioxide (SO_2) emissions from nearby industries. Remarkably, the sulfate content in the groundwater was found to be about ten orders of magnitude lower than that of the rainwater. During our fieldwork, we also noted a foul smell of rotten eggs in three borehole samples within the northern zone, which indicated the presence of hydrogen sulfide (H_2S). The amount of H_2S remaining in the solution depends strongly on the amount of Fe (II) in the groundwater solution [35]. Appelo and Postma [35] emphasized that H_2S can undergo additional reactions with Fe-oxide surfaces, thereby leading to the formation of iron sulfide minerals, such as pyrite, which aligns with our models predicting pyrite as a secondary mineral. These findings suggest that reactions in the soil and the unsaturated zones play a significant role in chemical evolution of the groundwater prior to recharge. We demonstrated that it is possible to calibrate the mineral assemblages using a reaction path model while taking extra hypotheses into account in the event that the presented combinatorial inverse model technique does not produce a reasonable outcome.

The weathering of silicate minerals controls the enrichment of major cations, including Na^+ , K^+ , Ca^{2+} , Mg^{2+} , and the anionic HCO_3^- in the groundwater system, with carbonate dissolution playing a subordinate role. Petrographic analysis of the outcrops indicated the predominance of silicate minerals, including plagioclase (albite and anorthite), muscovite (as K-mica), K-feldspar, and biotite (as phlogopite), which was further supported by our inverse equilibrium simulations, which revealed their dominant contribution to the groundwater system. With this in mind, the water–rock interactions along the flow path will likely result from the reactions involving these minerals in the presence of water. Manu et al. [1] and Tay et al. [9] used a combined interpretation of ion plots and principal component analysis and showed that groundwater evolution in the Pra Basin is driven by the weathering of silicate minerals.

The results of the reaction path modelling indicate that the chemical behaviour of Na^+ along the flow path is mainly controlled by albite weathering. This finding is supported by the predicted mineral assemblages from the combinatorial inverse modelling, which indicate albite dissolution in the north and central zones. In the case of Ca^{2+} , our model results indicate that the dissolution of anorthite mainly controls its occurrence in the groundwater. The alteration of biotite into chlorite, as observed in the thin section analysis and further confirmed by the combinatorial inverse model along Flowpath III (southern zone), along with the consistent occurrence of chlorite in the 50 best-matched equilibrium models, play a crucial role in determining the fate of dissolved potassium. Magnesium appears to be the most challenging element in the system, which showed the greatest variation from the median concentration despite being within the reported compositional range. The

dissolution of primary biotite (as phlogopite) identified by the petrographic analysis is the most likely source that could explain the release of Mg^{2+} into the groundwater. However, just a handful of our equilibrium models predicted its occurrence, thus implying that additional processes, such as cation exchange, may contribute to the chemical behaviour of the Mg^{2+} in the aquifer system.

In relation to dissolved Fe, our equilibrium models consistently suggested the presence of $Fe(OH)_3$ as a chemically relevant mineral controlling the behaviour of Fe in the system. This is evident from its frequent occurrence among the overall best-matched simulations. On the other hand, chloride and sulfate exhibited conservative behaviour along the flow path from the recharge to the discharge point, which can be attributed to the absence of halite or sulfate-containing minerals in the area. While sulfate could potentially be released from pyrite oxidation, our equilibrium models predicted pyrite as a secondary mineral, thus aligning with the field observations.

In contrast, the influence of carbonate mineral dissolution on groundwater chemistry was minimal, as demonstrated by our models. Although calcite is present in the terrain, based on our petrographic analysis, it rarely occurred in our simulated results, thus suggesting that it is a secondary mineral in the groundwater system. Our results are consistent with previous studies [1,9,11,41,42] and provide a strong conclusion that the weathering of silicate minerals is the primary factor driving groundwater chemistry in the Pra Basin.

The water chemistry in the Pra Basin is heterogeneous. A recent cluster analysis performed by Manu et al. [1] revealed that the hydrochemical variation was indistinguishable based on geology, which led to the division into three clusters based on elevation differences. Hence, this makes understanding the factors controlling hydrochemistry quite difficult. To address this challenge, we had to work with an average description, and we assumed the median concentrations of the clusters as representations of the chemical composition. Our modelling results show that some aqueous components, such as K^+ , Ca^{2+} , and Mg^{2+} , differed significantly from the target median ion composition. Despite these significant deviations from the median composition, all the simulated aqueous components fell within the range of the observed compositional values. This suggests that, even based on an averaged heterogeneous water composition and scarce information about the mineralogy, distinct and concise reaction paths can be determined.

By leveraging aquatic chemistry, we have been able to bridge the knowledge gap and produce plausible predictions of mineralogy controlling the chemical evolution of the groundwater on a large basin scale. Even though an averaged water composition was used, the inverse models could come up with distinct “best” mineral assemblages reflecting the underlying geology. Our models produced plausible mineral assemblages, which varied across different zones of the flow path. However, we must acknowledge that we only collected a few outcrop samples at random locations in the terrain, which limited our knowledge of the minerals in the area. Therefore, we inferred the secondary minerals based on our understanding of possible weathering products of primary minerals, such as plagioclase, albite, and K-feldspar, without requiring detailed analysis. This allowed us to constrain the mineral phases in our model setup and predict their likely formation, which aligned with the observed composition. Overall, we conclude that knowing about aquatic chemistry is more critical than accurate knowledge of mineralogy, because it is easier to sample and measure.

A conceptual hydrogeochemical model for the Pra Basin was constructed based on the results of the combinatorial inverse and reaction path models (Figure 7). It shows the principal assumption that the groundwater flows from a higher elevation in the northern zone through the centre of the basin to a lower elevation in the southern zone, which follows the topography. Rainwater is the main source of groundwater recharge, and its chemistry is affected by industrial activities in the area. The acidity of the rainwater is potentially controlled by SO_2 from fossil fuel combustion, which oxidizes and precipitates as dilute sulfuric acid. The chemistry of the rainwater is altered by evaporation, thus leading to changes in ion concentration and a subsequent decrease in the pH. Organic matter

degradation is the primary mechanism driving sulfate/sulfide content in the groundwater. We assumed that, as water infiltrates the unsaturated zone, the equilibration of secondary hematite and kaolinite represents the “limiting concentration” for the unknown sources of Fe and Al. Groundwater chemistry changes along the subsurface flow path from the recharge to the discharge zones due to water–rock interactions. The influence of the vertical flow along the flow path has a negligible impact on the chemical composition of the groundwater. The groundwater in the northern, central, and southern zones could be reproduced under local thermodynamic equilibrium conditions. In the northern zone (recharge area), the dissolution of albite and $\text{Fe}(\text{OH})_3$, along with the precipitation of chalcedony, are the most likely reactions affecting the dissolved ions. Similarly, the most probable reactions in the central zone are the dissolution of albite and $\text{Fe}(\text{OH})_3$, as well as the precipitation of plagioclase and chalcedony. In the southern zone, which serves as the discharge area, anorthite has been observed to dissolve, while chalcedony and chlorite precipitate. These reaction patterns highlight the key processes occurring in each zone to maintain the chemical balance of the groundwater system.

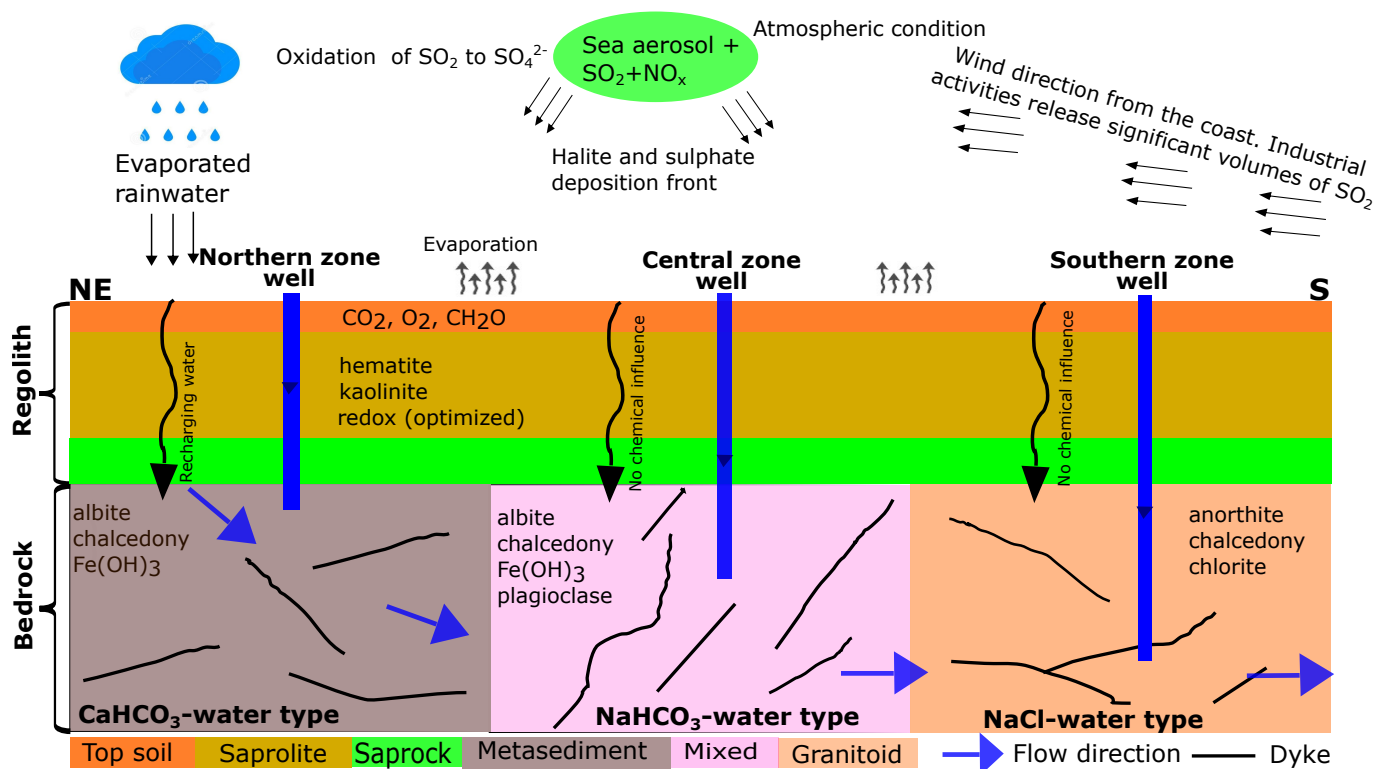


Figure 7. Conceptual model of hydrogeochemical evolution and groundwater flow path in the crystalline basement aquifer system of the Pra Basin in Ghana. Groundwater is assumed to flow from the northeast to the south of the basin.

Model Limitations

The use of average groundwater compositions to represent different zones along a flow regime and thermodynamic equilibrium assumptions to generate realistic mineral assemblages may have drawbacks. Because the hydrochemical data in this study exhibits a high degree of variability, employing the average water composition may oversimplify the variability in each of the three zones. As a result, if the water composition range is too wide, there may be significant differences between the simulated and observed values.

In addition, since some reactions are likely to be kinetically controlled, the model assumption based on thermodynamic equilibrium may not accurately reflect the true natural state. This could alter the predicted mineral assemblages by affecting mineral dissolution and precipitation rates.

It is important to mention that the modelling approach used in this study considered pure phases from a stoichiometric perspective. However, this can result in discrepancies for certain elements, particularly in the case of clay minerals such as chlorite.

Another drawback of our model is the absence of cation exchange, which can have a considerable impact on the amounts of Na^+ , K^+ , Ca^{2+} , and Mg^{2+} in the simulated groundwater. We found significant differences in the concentrations of K^+ , Ca^{2+} , and Mg^{2+} in the final simulated groundwater solution, especially in the southern zone. These disparities may be linked to the influence of cation exchange, which likely controls the amount of these minerals in the aquifer system.

5. Conclusions

The present study successfully implemented sequential geochemical numerical simulations to understand the chemical evolution of groundwater in a heterogeneous basin-scale environment. A combinatorial inverse modelling approach was employed to determine the most likely mineral assemblage in equilibrium. The mineral assemblages were further calibrated through reaction path modelling to elucidate the changes in groundwater composition along the flow path. Our findings allow for the following conclusions:

1. The plausible mineral assemblages that best explain the chemical composition of the groundwater in the Pra Basin have been identified. These mineral assemblages, including albite, chalcedony, and $\text{Fe}(\text{OH})_3$ for the northern zone, albite, chalcedony, $\text{Fe}(\text{OH})_3$, and plagioclase for the central zone, and anorthite, chalcedony, and chlorite for the southern zone, were found as plausible mineral assemblages governing the dissolved ions in the groundwater, and these assemblages align with petrographic information from outcrops.
2. Groundwater chemistry is governed by silicate mineral weathering, with the dissolution of carbonate minerals playing a subordinate role. Based on the results of the combinatorial inverse modelling, it is clear that the majority of the mineral phases commonly found in the models are silicates, including primary albite, anorthite, plagioclase, phlogopite, K-mica, and K-feldspar, as well as secondary chlorite, kaolinite, chalcedony, and quartz. Our model results rarely predicted the occurrence of calcite in the 50 best-matched solutions, thus suggesting that carbonate minerals have less impact on the basin's groundwater composition.
3. The degradation of organic matter primarily controls the reduction in sulfate in the groundwater. This is supported by the observed foul smell of rotten eggs in some of the sampled wells, which indicated the presence of hydrogen sulfide (H_2S). Additionally, our modelling results indicate the formation of pyrite, which occurs when H_2S produced from organic matter degradation reacts with the dissolved $\text{Fe}(\text{II})$ in the groundwater.
4. The simulation results revealed that accurate knowledge of aquifer mineralogy is less important than aquatic chemistry, which fortunately is easier to sample and measure. Average water compositions are sufficient to successfully “bridge” the knowledge gap on the large basin scale to come up with distinct “best” mineral assemblages. By leveraging aquatic chemistry, we were able to produce plausible predictions of the mineralogy on a large basin scale with limited knowledge of the mineral compositions obtained from the petrographic analysis of some outcrops in the study area.
5. Equilibrium-based thermodynamic concepts of water–rock interactions were used to quantify the observed hydrochemical variations. However, we acknowledge that the northern zone (Flowpath I), which is assumed to be the recharge area, required additional hypotheses to match the observed composition, thus pointing towards kinetic effects during water–rock interactions. The results of our models emphasized the equilibration of the initial rainwater with the partial pressure of CO_2 ($10^{-1.7}$ atm), followed by the subsequent equilibration of the resulting solution with kaolinite, hematite, and redox optimization ($\text{pe} = 3.5$). Additionally, the calibrated model accounted for the reaction with 4.0×10^{-4} moles of organic matter.

6. A combined interpretation of the combinatorial inverse and reaction path models allowed for the successful development of a conceptual framework of the hydrochemical evolution for the Pra Basin. Based on our models, the main source of groundwater recharge in the Pra Basin is rainwater that has undergone some degree of evaporation. Our hypothesis of geochemical equilibrium among specific mineral assemblages explains the chemical evolution of groundwater from the point of recharge to the point of discharge. Our modelling results indicate that specific reactions play a crucial role in controlling the groundwater evolution in different zones of the basin. In the northern zone, the equilibration of albite, $\text{Fe}(\text{OH})_3$, and chalcedony is highlighted as the primary reaction influencing the groundwater chemistry. The equilibration involving albite, $\text{Fe}(\text{OH})_3$, plagioclase, and chalcedony is identified as an important factor for the central zone. In the southern zone, the equilibrium of anorthite, chalcedony, and chlorite is significant for understanding the groundwater composition.

Overall, our study provides a concept of the chemical evolution of groundwater in a basin-scale environment. Our findings have implications for the groundwater resource management in the Pra Basin, and our numerical modelling workflow can be applied in similar regions with large heterogeneity in water chemistry and limited knowledge of aquifer mineralogy.

Author Contributions: Conceptualization, E.M. and M.K.; methodology, E.M., M.K. and M.D.L.; software, E.M. and M.D.L.; validation, E.M. and M.D.L.; formal analysis, E.M.; investigation, E.M.; writing—original draft preparation, E.M.; writing—review and editing, E.M., M.D.L. and M.K.; visualization, E.M.; supervision, M.K. All authors have read and agreed to the published version of the manuscript.

Funding: This publication has been supported by the funding programme “Open Access Publikationskosten” Deutsche Forschungsgemeinschaft (DFG, German Research Foundation)—Project Number 491075472. The first author was funded by the German Academic Exchange Service (DAAD) with the program funding number 57460308.

Data Availability Statement: Datasets related to this article can be found at <https://doi.org/10.5880/GFZ.3.4.2023.002>, accessed on 25 March 2023. The R code used to perform the combinatorial inverse models can be provided upon request to the corresponding author.

Acknowledgments: This study is part of the first author’s doctoral thesis. He would like to express his greatest appreciation to the German Academic Exchange Service (DAAD) for funding his stay in Germany. We also thank the Water Research Institute of Ghana for their assistance during the field campaigns. Our special thanks go to Thomas Kempka of GFZ German Research Centre for Geosciences for his comments and assistance throughout the research process. We also acknowledge the support from Kwabina Ibrahim from the Department of Earth Science at the University of Ghana (Legon) for the assistance provided during the field campaigns.

Conflicts of Interest: The authors declare no conflict of interest.

Appendix A

Below is the list of mineral phases, their governing equations, and the thermodynamic equilibrium constants used in the combinatorial inverse and reaction path modelling. The data were adopted from the `phreeqc.dat` thermodynamic database. The fixed stoichiometry plagioclase equation and equilibrium constant was derived by weighted averaging of the sodium plagioclase (albite) and the calcium plagioclase (anorthite) using the observed geochemical data from the available outcrops.

Table A1. List of additional phases included in the phreeqc.dat database for the simulations.

Mineral	Chemical Equation	log ₁₀ K ₂₅
Phlogopite	$\text{KMg}_3(\text{AlSi}_3)\text{O}_{10}(\text{OH})_2 + 10 \text{H}^+ = 1 \text{Al}^{+3} + 1 \text{K}^+ + 3 \text{Mg}^{+2} + 3 \text{H}_4\text{SiO}_4$	41.08
Plagioclase	$\text{Na}_{0.62}\text{Ca}_{0.38}\text{Al}_{1.38}\text{Si}_{2.62}\text{O}_8 + 8\text{H}_2\text{O} = 0.62\text{Na}^+ + 0.38\text{Ca}^{+2} + 1.38\text{Al}(\text{OH})_4^- + 2.62\text{H}_4\text{SiO}_4$	−18.65
Organic matter	$\text{CH}_2\text{O} + \text{H}_2\text{O} = 4 \text{e}^- + 4 \text{H}^+ + \text{CO}_2$	4.80

References

- Manu, E.; De Lucia, M.; Kühn, M. Hydrochemical characterization of groundwater in the crystalline basement aquifer system in the Pra Basin (Ghana). *Water* **2023**, *15*, 1325. [\[CrossRef\]](#)
- Tay, C.K.; Kortatsi, B.K.; Hayford, E.; Hodgson, I.O. Origin of major dissolved ions in groundwater within the Lower Pra Basin using groundwater geochemistry, source-rock deduction and stable isotopes of 2 H and 18 O. *Environ. Earth Sci.* **2014**, *71*, 5079–5097. [\[CrossRef\]](#)
- Affum, A.O.; Dede, S.O.; Nyarko, B.J.B.; Acquah, S.O.; Kwaansa-Ansah, E.E.; Darko, G.; Dickson, A.; Affum, E.A.; Fianko, J.R. Influence of small-scale gold mining and toxic element concentrations in Bonsa river, Ghana: A potential risk to water quality and public health. *Environ. Earth Sci.* **2016**, *75*, 178. [\[CrossRef\]](#)
- Bempah, C.K.; Ewusi, A. Heavy metals contamination and human health risk assessment around Obuasi gold mine in Ghana. *Environ. Monit. Assess.* **2016**, *188*, 261. [\[CrossRef\]](#)
- Armah, F.A.; Quansah, R.; Luginaah, I. A systematic review of heavy metals of anthropogenic origin in environmental media and biota in the context of gold mining in Ghana. *Int. Sch. Res. Not.* **2014**, *2014*, 252148. [\[CrossRef\]](#)
- Golow, A.; Mingle, L. Mercury in river water and sediments in some rivers near Dunkwa-on-Offin, an alluvial goldmine, Ghana. *Bull. Environ. Contam. Toxicol.* **2003**, *70*, 0379–0384. [\[CrossRef\]](#)
- Amonoo-Neizer, E.H.; Amekor, E. Determination of total arsenic in environmental samples from Kumasi and Obuasi, Ghana. *Environ. Health Perspect.* **1993**, *101*, 46–49. [\[CrossRef\]](#)
- Loh, Y.S.A.; Fynn, O.F.; Manu, E.; Afrifa, G.Y.; Addai, M.O.; Akurugu, B.A.; Yidana, S.M. Groundwater-surface water interactions: application of hydrochemical and stable isotope tracers to the lake bosumtwi area in Ghana. *Environ. Earth Sci.* **2022**, *81*, 518. [\[CrossRef\]](#)
- Tay, C.K.; Hayford, E.; Hodgson, I.O.; Kortatsi, B.K. Hydrochemical appraisal of groundwater evolution within the Lower Pra Basin, Ghana: A hierarchical cluster analysis (HCA) approach. *Environ. Earth Sci.* **2015**, *73*, 3579–3591. [\[CrossRef\]](#)
- Banoeng-Yakubo, B.; Yidana, S.M.; Anku, Y.; Akabzaa, T.; Asiedu, D. Water quality characterization in some Birimian aquifers of the Birim Basin, Ghana. *KSCE J. Civ. Eng.* **2009**, *13*, 179–187. [\[CrossRef\]](#)
- Loh, Y.S.A.; Addai, M.O.; Fynn, O.F.; Manu, E. Characterisation and quality assessment of surface and groundwater in and around Lake Bosumtwi impact craton (Ghana). *Sustain. Water Resour. Manag.* **2021**, *7*, 1–18. [\[CrossRef\]](#)
- Apollaro, C.; Fuoco, I.; Bloise, L.; Calabrese, E.; Marini, L.; Vespasiano, G.; Muto, F. Geochemical modeling of water-rock interaction processes in the Pollino National Park. *Geofluids* **2021**, *2021*, 6655711. [\[CrossRef\]](#)
- Elango, L.; Kannan, R. Rock–water interaction and its control on chemical composition of groundwater. *Dev. Environ. Sci.* **2007**, *5*, 229–243.
- Plummer, L.N.; Prestemon, E.C.; Parkhurst, D.L. An interactive code (NETPATH) for modeling net geochemical reactions along a flow path, version 2.0. *Water-Resour. Investig. Rep.* **1994**, *94*, 4169.
- Parkhurst, D.L.; Appelo, C. User's guide to PHREEQC (Version 2): A computer program for speciation, batch-reaction, one-dimensional transport, and inverse geochemical calculations. *Water-Resour. Investig. Rep.* **1999**, *99*, 312.
- Parkhurst, D.L. *User's Guide to PHREEQC: A Computer Program for Speciation, Reaction-Path, Advective-Transport, and Inverse Geochemical Calculations*; US Geological Survey; US Department of the Interior: Washington, DC, USA, 1995; pp. 95–4227.
- Bethke, C.M. *Geochemical and Biogeochemical Reaction Modeling*; Cambridge University Press: Cambridge, UK, 2022.
- Xu, T.; Sonnenthal, E.; Spycher, N.; Pruess, K. *TOUGHREACT User's Guide: A Simulation Program for Non-Isothermal Multiphase Reactive Geochemical Transport in Variable Saturated Geologic Media*; Technical Report; Lawrence Berkeley National Lab. (LBNL): Berkeley, CA, USA, 2004.
- De Lucia, M.; Kühn, M. Geochemical and reactive transport modelling in R with the RedModRphree package. *Adv. Geosci.* **2021**, *56*, 33–43. [\[CrossRef\]](#)
- Dzignbodi-Adjimah, K. Geology and geochemical patterns of the Birimian gold deposits, Ghana, West Africa. *J. Geochem. Explor.* **1993**, *47*, 305–320. [\[CrossRef\]](#)
- Kesse, G. *The Manganese Ore Deposits of Ghana*; Ghana Geological Survey Bulletin: Accra, Ghana, 1976; Volume 44.
- Kesse, G.O. *The Mineral and Rock Resources of Ghana*; Ghana Geological Survey Bulletin: Accra, Ghana, 1985.
- Leube, A.; Hirdes, W.; Mauer, R.; Kesse, G.O. The early Proterozoic Birimian Supergroup of Ghana and some aspects of its associated gold mineralization. *Precambrian Res.* **1990**, *46*, 139–165. [\[CrossRef\]](#)
- Nyame, F.K. Origins of Birimian (ca 2.2 Ga) mafic magmatism and the P aleoproterozoic greenstone belt metallogeny: A review. *Isl. Arc* **2013**, *22*, 538–548. [\[CrossRef\]](#)

25. Manu, J.; Hayford, E.; Anani, C.; Kutu, J.M.; Armah, T. Aspects of the chemical composition of the Birimian gold fluid. *J. Earth Sci. Geotech. Eng.* **2013**, *3*, 87–106.
26. Banoeng-Yakubo, B.; Yidana, S.; Ajayi, J.; Loh, Y.; Asiedu, D. Hydrogeology and groundwater resources of Ghana: A review of the hydrogeology and hydrochemistry of Ghana. In *Potable Water and Sanitation*; McMann, J.M., Ed.; Nova Science: New York, NY, USA, 2010; Volume 142.
27. Yidana, S.M.; Banoeng-Yakubo, B.; Sakyi, P.A. Identifying key processes in the hydrochemistry of a basin through the combined use of factor and regression models. *J. Earth Syst. Sci.* **2012**, *121*, 491–507. [[CrossRef](#)]
28. Leube, A.; Hirdes, W. The early Proterozoic (Birimian and Tarkwaian) of Ghana and some aspects of its associated gold mineralizations. *Ext. Abstr. Geocongress* **1986**, *86*, 315–319.
29. Ganyaglo, S.Y.; Banoeng-Yakubo, B.; Osae, S.; Dampare, S.B.; Fianko, J.R.; Bhuiyan, M.A. Hydrochemical and isotopic characterisation of groundwaters in the eastern region of Ghana. *J. Water Resour. Prot.* **2010**, *2*, 199. [[CrossRef](#)]
30. Manu, E.; Vieth-Hillebrand, A.; Rach, O.; Schleicher, A.M.; Trumbull, R.; Stammeier, J.A.; Gottsche, A.; Kühn, M. Hydrochemistry and stable oxygen ($\delta^{18}\text{O}$) and hydrogen ($\delta^2\text{H}$) isotopic composition of surface water and groundwater and mineralogy, in the Pra Basin (Ghana) West Africa. *GFZ Data Services*. **2023**. [[CrossRef](#)]
31. Akoto, O.; Darko, G.; Nkansah, M. Chemical composition of rainwater over a mining area in Ghana. *Int. J. Environ. Res.* **2011**, *5*, 847–854.
32. Akoto, O.; Adiyiah, J. Chemical analysis of drinking water from some communities in the Brong Ahafo region. *Int. J. Environ. Sci. Technol.* **2007**, *4*, 211–214. [[CrossRef](#)]
33. Thyne, G.; Güler, C.; Poeter, E. Sequential analysis of hydrochemical data for watershed characterization. *Groundwater* **2004**, *42*, 711–723. [[CrossRef](#)]
34. Circone, S.; Navrotsky, A. Substitution of [6, 4] Al in phlogopite: High-temperature solution calorimetry, heat capacities, and thermodynamic properties of the phlogopite-eastonite join. *Am. Mineral.* **1992**, *77*, 1191–1205.
35. Appelo, C.; Postma, D. *Geochemistry, Groundwater and Pollution*, 2nd ed.; Rotterdam, B., Ed.; CRC Press: London, UK, 2005.
36. Pitkaenen, P.; Luukkonen, A.; Ruotsalainen, P.; Leino-Forsman, H.; Vuorinen, U. *Geochemical Modelling of Groundwater Evolution and Residence Time at the Kivetty Site*; Technical Report; Posiva Oy: Eurajoki, Finland, 1998.
37. Asiedu, D.K.; Dampare, S.B.; Sakyi, P.A.; Banoeng-Yakubo, B.; Osae, S.; Nyarko, B.J.B.; Manu, J. Geochemistry of Paleoproterozoic metasedimentary rocks from the Birim diamondiferous field, southern Ghana: Implications for provenance and crustal evolution at the Archean-Proterozoic boundary. *Geochem. J.* **2004**, *38*, 215–228. [[CrossRef](#)]
38. Adiaffi, B.; Marlin, C.; Coulibaly, Y.; Oga, Y.M.S.; Pichon, R. Hydrogeochemistry of Bedrock Groundwater in SE Ivory Coast. *Int. J. Emerg. Technol. Adv. Eng.* **2016**, *6*, 1–14.
39. Appelo, C.; Dimier, A. *Geochemistry, Groundwater and Pollution: Learning by Modeling*; US Federal Agency Workshop: Albuquerque, NM, USA, 2004.
40. Freeze, R.A.; Cherry, J. *Groundwater*; Prentice-Hall, Inc.: Englewood Cliffs, NJ, USA, 1979.
41. Tay, C.K. Hydrochemistry of groundwater in the Savelugu–Nanton District, northern Ghana. *Environ. Earth Sci.* **2012**, *67*, 2077–2087. [[CrossRef](#)]
42. Okofo, L.B.; Anderson, N.A.; Bedu-Addo, K.; Armoo, E.A. Hydrochemical peculiarities and groundwater quality assessment of the Birimian and Tarkwaian aquifer systems in Bosome Freho District and Bekwai Municipality of the Ashanti Region, Ghana. *Environ. Earth Sci.* **2021**, *80*, 818. [[CrossRef](#)]

Disclaimer/Publisher’s Note: The statements, opinions and data contained in all publications are solely those of the individual author(s) and contributor(s) and not of MDPI and/or the editor(s). MDPI and/or the editor(s) disclaim responsibility for any injury to people or property resulting from any ideas, methods, instructions or products referred to in the content.